A Compact Laser-Steering End-Effector for Transoral Robotic Surgery

Simon A. Bothner*, Peter A. York*, *Student Member, IEEE*, Phillip C. Song, and Robert J. Wood, *Fellow, IEEE*

***Abstract*— Laryngeal cancer treatments, while curative, often lead to voice impairment. Minimally invasive surgical methods that facilitate greater preservation of healthy tissue have recently emerged, but they are still limited in important ways. In this work, we describe a device that combines the advantages of the two primary minimally invasive approaches: the high quality incision and reduced post-operative pain achievable with transoral laser microsurgery and the superior visualization and tissue manipulability afforded by transoral robotic surgery. Our $11\,\mathrm{mm}$ diameter scanning system connects to focusing optics and a fiber optic laser source and can direct a laser beam across a $18 \times 10\,\mathrm{mm}$ plane with controllable trajectories at speeds up to $7\,\mathrm{m/s}$. We describe its design and benchtop validation and present avenues for further development within a clinical environment. While oncological treatment is a natural first application area for this technology, we anticipate that it may also yield important benefits for the minimally invasive treatment of benign laryngeal diseases.**

I. Introduction

Over 30,000 people in the U.S. were diagnosed in 2018 with a cancer of the pharynx or larynx [1], resulting in 6,000 deaths. These cancers are notable for their deleterious effect on quality of life; their symptoms, including dysphagia and voice impairment, often lead to depression and social isolation, and curative treatments often exacerbate these functional maladies [2]. Incidence, historically driven by the smoking of tobacco, is increasingly driven by human papillomavirus, resulting in a historically young patient population even more concerned with long-term functional outcomes [3].

Thus, there is significant need for curative treatment methods for these cancers that enable post-treatment organ function. Partial or full organ removal via open surgery represents one extreme: the near guarantee of excellent oncological results at the expense of functional outcomes. Nonoperative methods, including induction chemotherapy, intensity modulated radiotherapy, and concurrent chemotherapy with radiotherapy, offer better functional outcomes than open surgery while achieving good oncological results. Such techniques are currently recommended for most laryngeal cancers [4]. However, within the last two decades, the perceived long-term morbidity and functional impairment

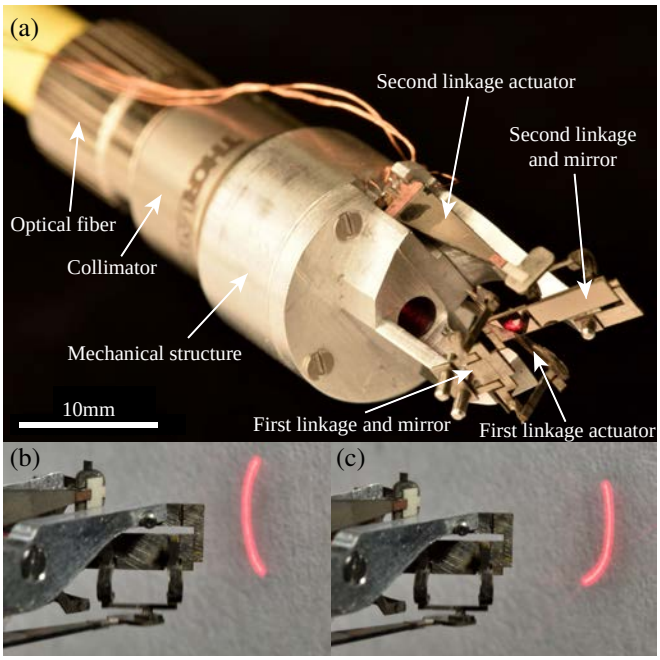

Fig. 1: (a) Laser scanning system for use in transoral robotic surgery. The device receives a fiber input and steers a focused beam onto the surgical plane. (b-c) Long exposure photographs demonstrating typical cut profiles used in laser-based tissue resection.

associated with radiotherapy have led some otolaryngologists to reexamine surgical techniques [5]. Minimally invasive methods are of particular interest, with a view toward greater preservation of healthy tissue and associated improvements in post-operative organ function relative to open surgery.

Transoral laser microsurgery (TLM), first described in 1972 [6], is the most mature minimally invasive approach. In TLM, a carbon dioxide laser is coupled to a surgical microscope and aimed through a laryngoscope, which provides line-of-sight access to the upper airway. The surgeon uses manual tools inserted through the laryngoscope to retract the lesion and uses a micromanipulator on the microscope to steer the laser beam to resect the diseased tissue. In advanced systems, the micromanipulator is motorized, allowing the surgeon to direct the laser along predetermined arcs and lines at precisely controlled speeds, resulting in very high quality incisions [7]. The most significant limitation of TLM is its line-of-sight constraint, which restricts both visualization and exposure. Moreover, the long, narrow laryngoscope makes the manual manipulation of tools required for retraction and suturing difficult.

To address these shortcomings, transoral robotic surgery (TORS) was developed in the mid 2000s [8], [9]. In TORS, flexible or wristed robotic manipulators are used in con-

* These authors contributed equally to this work.

Simon A. Bothner is with Ecole Polytechnique Federale de Lausanne, Lausanne, Switzerland, simon@bothner.com

Peter A. York and Robert J. Wood are with the John A. Paulson School of Engineering and Applied Sciences and the Wyss Institute for Biologically Inspired Engineering, Harvard University, Cambridge, MA USA, pyork@g.harvard.edu, rjwood@eecs.harvard.edu

Phillip C. Song is with the Division of Laryngology, Mass Eye and Ear, Boston, MA, USA, Phillip_Song@meei.harvard.edu

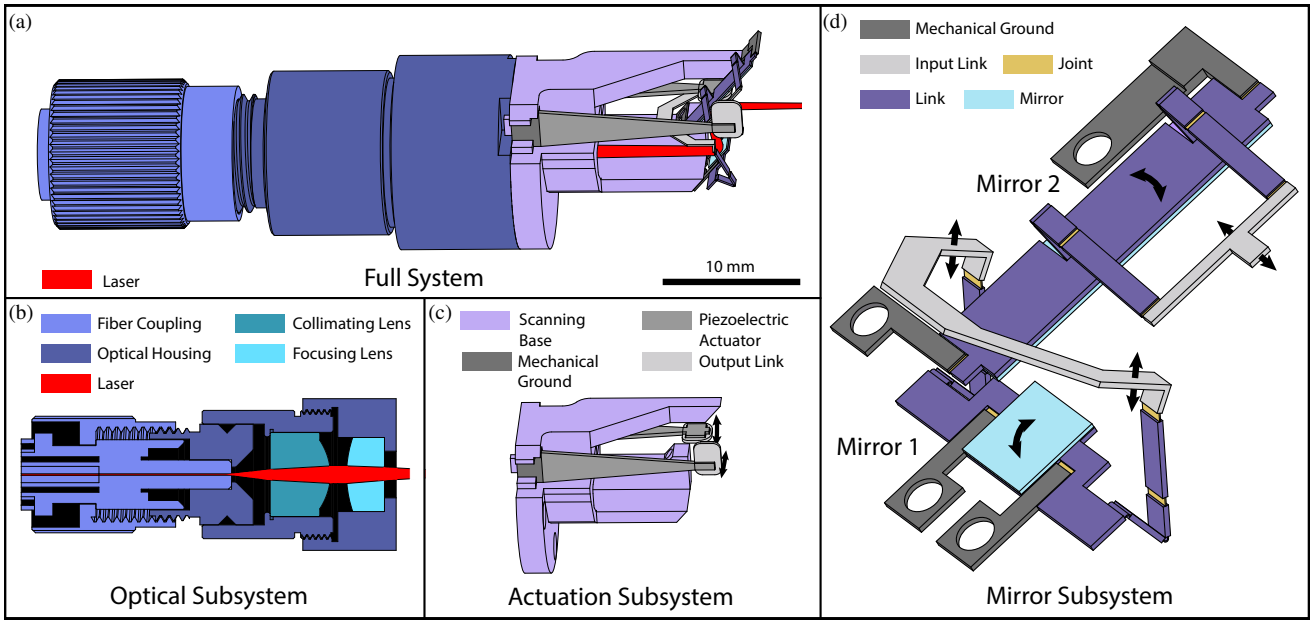

Fig. 2: (a) 3D drawing of the laser-scanning end effector defining the location of key subsystems. (b) Optical subsystem, which connects a fiber optic source to the laser scanner. (c) Actuation subsystem, consisting of piezoelectric bending actuators and a rigid mechanical base that aligns the optics with the rest of the device. (d) Mirror subsystem containing motion transmissions and flat mirrors.

junction with endoscopic vision systems, providing superior visualization and tissue manipulability at the surgical site. The da Vinci multi-port and da Vinci single port systems (Intuitive Surgical Inc, Sunnyvale, CA) and the Flex Robotic System (Medrobotics, Raynham, MA, USA) are currently in clinical use [10].

However, TORS remains deficient to TLM in at least one key respect: in TORS, electrocautery is primarily employed for resection, which leads to greater post-operative pain and longer recovery times than in similar procedures conducted with TLM [11]. With the recent development of hollow core fibers capable of delivering carbon dioxide lasers through flexible instruments, the use of lasers in TORS is expected to increase [12], which should mitigate this problem to some degree. However, fiber-based lasers must be held and manually manipulated by robotic tools, and thus lack the spatial repeatability, precision, and speed of free-beam scanning systems. This implies that incision quality suffers relative to the free-beam systems used for TLM. Free-beam systems have the additional benefit of leaving the surgical site clear for exposure and visualization of margins.

Thus, there is an opportunity to capture the benefits of both TLM and TORS, by creating a laser scanning system that operates at the end of a robot manipulator. This configuration would enable more precise incisions and tighter margins than achievable with existing laser or electrocautery tools. Moreover, by moving the laser fiber inside the robot manipulator, it may be possible to relax some of the constraints on the fiber's design and use; currently available CO2-laser fibers are expensive (around $1000) and single-use. In the proceeding sections, we will describe a prototype device for enabling this TLM/TORS hybrid paradigm.

II. Design

Design requirements are derived from the prospective surgical environment. We choose a target field of view of $10 \times 20\,\mathrm{mm}$, in accordance with the nominal size of the vocal folds. In order to leave room for retraction tools, visualization, and illumination, an upper bound of $11\,\mathrm{mm}$ on device diameter was chosen. To balance the needs for visualization and the manipulation of tissue while minimizing the angle of view of the scanning system, we chose a standoff distance of $20\,\mathrm{mm}$. Lastly, we chose a target spot size of $250\,\mu\mathrm{m}$ and a target surface speed of $100\,\mathrm{mm/s}$, both in accordance with the scanning systems used in TLM [13].

A. State of the Art

A number of prototype endoscopic devices have been developed for minimally invasive laser scanning tasks, each with a different approach to the challenging design problem. Patel used DC motor-driven Risley prisms as the beam steering method to achieve moderate scanning speeds ($471\,\mathrm{mm/s}$) and a large field of view ($75\,\mathrm{mm}$ diameter) at $75\,\mathrm{mm}$ working distance, but the device is quite bulky ($17\,\mathrm{mm}$ diameter) and uses rotary transmission components that are challenging to further downscale [14]. Ferhanoglu, et al. used piezoelectric actuators to directly bend an optical fiber, achieving a high laser speed ($500\,\mathrm{mm/s}$ at $3.5\,\mathrm{mm}$ working distance) in a thin device profile ($5\,\mathrm{mm}$ diameter), but the field of view ($250 \times 250\,\mu\mathrm{m}$) suffered as a result [15]. Acemoglu, et al. used electromagnets to bend a fiber, which increased the range of motion to $3 \times 3\,\mathrm{mm}$, but in doing so sacrificed laser speed ($94\,\mathrm{mm/s}$ at $30\,\mathrm{mm}$ working distance) [16]. Lastly, the FEMTO-ST Institute developed a system that uses off-the-shelf piezoelectric linear actuators to articulate a silicon mirror held on a tip-tilt stage, which achieves a $20 \times 20\,\mathrm{mm}$

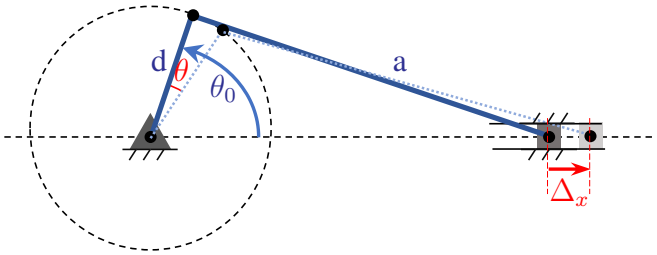

	d [mm]	a [mm]	θ_0 [°]
Mirror 1	0.9	2	70
Mirror 2	0.6	2	75

Fig. 3: The crank-slider transmission motion schematically represented with chosen design values shown in the table.

field of view but relies on an unwieldy external mirror to reflect back on to the tip-tilt stage; also, the cutting speed is not provided [17].

B. System Concept

In our approach, shown in Fig. 2, we leverage newly-developed microfabrication techniques [18] to create miniature mechanical transmissions that convert the quasi-linear motions of high-bandwidth piezoelectric bending actuators [19] into rotational motions that are used to orient mirrors. Our device contains two such actuator-transmission-mirror combinations, situated orthogonally, such that the two actuation inputs correspond to ablation in orthogonal directions on the target tissue. Light is transmitted to the laser scanner using an optical fiber and then fed into a collimating and a focusing lens assembly. The focused beam is then steered by rotating the two mirrors using crank-slider transmissions to convert the linear actuator movement to the desired rotational mirror movement. The scanning base provides a mechanical ground for the actuators and the transmissions and guarantees precise alignment between the optical subsystem and the mirror subsystem.

C. Optical Design

Many different lasers are used in laryngeal surgery, including CO_2, KTP, and diode [20], [21]. While CO_2 lasers are the preferred choice in many contexts, optical fibers transmitting this wavelength at high power tend to have a large core diameter, which implies a spot size that would exceed our design requirements. We therefore designed our device to be used with a diode laser that can be transmitted at high power (60 W) through a 35 µm core fiber (Nufern PM780-HP). For this prototype, however, we validated its mechanics with a low-power fiber optic inspection laser and left integration with the high-powered laser to future work.

We chose a 6.17 mm focal length collimator and a 38.1 mm focusing lens, which should yield a 210 µm spot diameter when combined with an optical fiber of 35 µm core diameter and a numerical aperture of 0.12. Both lenses are aspherical plano-convex to reduce aberrations. We chose mirror sizes of 2×2 mm and 2×5 mm with 40° initial angles, which were chosen in accordance with the kinematic analysis described below. We chose to use an off-the-shelf factory-aligned fiber-coupled collimator (Thorlabs' F110 FC-633) to simplify integration at the expense of increasing the size of this prototype.

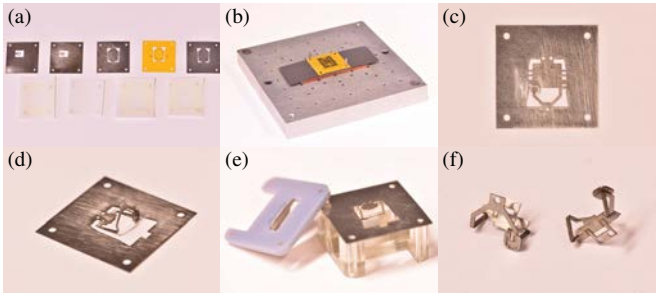

Fig. 4: Linkage manufacturing process. (a) Individual layers of rigid, flexible, and adhesive materials are cut using laser micromachining. (b) Layers are pin aligned and laminated using heat and pressure. (c) Further laser micromachining reveals the structure of the linkage. (d) After assembly tabs are released, the linkage structure is partially deployed. (e) A 3D-printed assembly jig is used to bend the linkage arms to their desired positions. (f) Final tabs are released and the linkages are ready to be integrated with the rest of the device.

D. Transmission design

Actuator lengths of 10.6 mm and 12.1 mm were chosen in order to achieve suitable displacement while not greatly lengthening the device. We assumed that the transmission stiffnesses would be approximately equal to the output stiffness of the actuators, implying a 50 % decrease in actuator deflection *in situ* versus free deflection. Under this assumption, the deflections of the actuators at 200 V (the upper limit on operating voltage to avoid damage to the piezoceramic actuator materials) are ±200 µm and ±220 µm, respectively.

Using the optical model described in Sec. IV and considering placement of the mirrors to minimize device diameter, we determined the desired ranges of motion to be ±10° for the first mirror and ±15° for the second. To generate these motions, the crank slider link lengths shown in Fig. 3 were chosen in accordance with the crank slider relation:

$$\theta = cos^{-1}\left(\frac{d^2 - a^2 + x^2}{2dx}\right) - \theta_0 \qquad (1)$$
$$x = x_0 + \Delta_x$$

where θ_0 is the initial angle of the crank slider, Δ_x is the actuator deflection, and x_o is the initial distance between the slider and the pivot. Of the two links, the length of the crank arm affects the output motion the most: the smaller it is, the larger the output movement is. Also of note is that the initial angle of the mechanism trades off symmetry for output amplitude. We chose the linkage configuration that achieved the desired range of motion while minimizing asymmetry. The fabricated linkages are shown in Fig. 4f.

III. Manufacturing

The manufacturing process used for fabricating the linkages is based on the approach developed in [18] and is shown in detail in Fig. 4. Individual layers of steel, polyimide, and acrylic adheisve are cut using an 7 W, 355 nm DPSS laser micromachining system (Oxford Lasers E Series) before

Symbol	Description
$e^i_j \in \mathbb{R}^3$	The jth basis vector of the ith coordinate system.
$\hat{v}^i_{jk} \in \mathbb{R}^3$	The unit vector directed from point p_j to point p_k, with respect to the ith frame.
$R^i_j \in SO(3)$	The orientation of the jth coordinate system with respect to the ith coordinate system.
$R_{i,\theta} \in SO(3)$	Elementary rotation about the i axis by angle θ.
H^i_j	Householder transformation about the jth basis vector of the ith coordinate system, expressed in local coordinates.

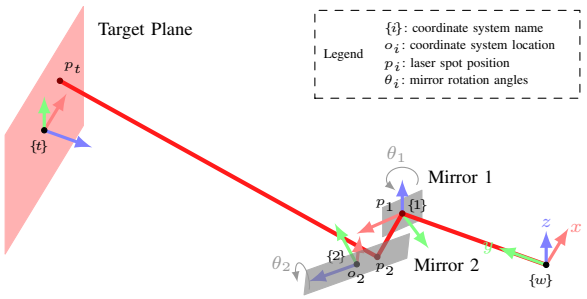

Fig. 5: Diagramatic representation of laser scanning system with key symbols defined.

being aligned and set into a heated press to bond the layers together. The bonded laminate is removed from the press, and preliminary release cuts are made. The laminates are then bent into their desired configurations; the first mirror transmission requires an assembly jig to bend it to the correct angles, while the second mirror makes use of the alignment pins used for stacking. The laminates are then locked in their aligned configuration using CA glue, and then final cuts are performed to release the desired degrees of freedom. Each linkage is set under a confocal microscope and its functional dimensions are measured to validate the process. The manufacturing of the linkages is very repeatable, with a standard deviation less than 4% of the desired value in all twelve linkages built, which corresponds to a 5% variation in linkage transmission ratio.

The small link lengths of the crank sliders make their assembly challenging, but by bending their physical arms backwards to create virtual links (as seen in Fig. 4e), their handling is made significantly easier. Moreover, by using this approach, the flexures' bending angles are zero at rest, which makes it easier to ensure they stay inside the elastic regime of deformation.

The linkages' ground connections are attached to a 7075 aluminum alloy base structure manufactured using a five-axis CNC machine (Bridgeport, Hardinge, Inc.). The mirrors are made by laser cutting an aluminum-sputtered 100 µm thick fused silica wafer. The aluminum deposition was conducted in a desktop sputtering chamber (Denton Vacuum Desktop Pro). A protective gel layer is added on the mirror to protect the reflective coating during the assembly. The linkages are then bonded to their respective actuators before being inserted into the mechanical structure and held in place with alignment pins and a press-fit plate. The actuator base and transmission ground linkages are then bonded to the mechanical structure with cyanoacrylate glue. Finally, fabrication is completed by carefully removing the protective gel layers from the mirrors.

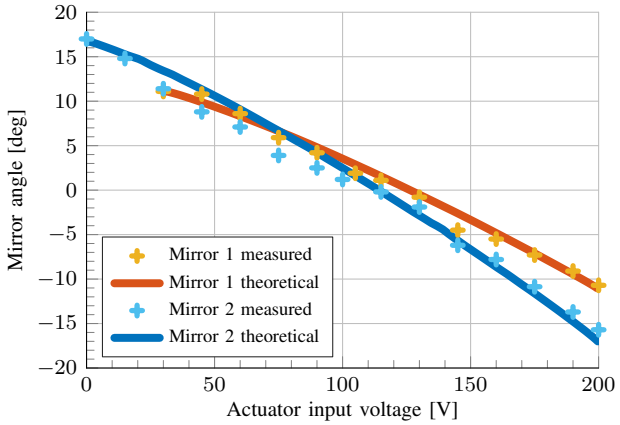

Fig. 6: Measurement of mirror angle as a function of actuator voltage. The overall trend is captured well by the model, with mean absolute errors of 0.6° and 1.2° for the first and second mirrors, respectively.

IV. Modeling

Given the mirror angles determined by the crank-slider relation (1), the laser spot location on the target plane can be found using the vector formulation of specular reflection. Symbols and geometric definitions used are given with the system schematic shown in Fig. 5. The orientations of the mirrors in 3D space are given by:

$$R^w_1 = R_{z,(\theta_1+\theta_{1,0})} \tag{2}$$
$$R^w_2 = R_{z,(\theta_{1,0}-\pi)} R_{y,-\pi/2} R_{z,\theta_2} \tag{3}$$

Where $\theta_{1,0}$ is a design variable denoting the initial orientation of the first mirror. Now, the ray reflected from the first mirror has direction:

$$\hat{v}^1_{12} = H^1_2 \left(R^w_1\right)^{-1} e^w_2 \tag{4}$$

And it intersects the second mirror after a distance d_{12}:

$$d_{12} = (o_2 - o_1)^T e^2_2 / \left(R^w_1 \hat{v}^1_{12}\right)^T e^2_2 \tag{5}$$

Thus, the location of the laser on the second mirror is given by:

$$p^w_2 = \begin{bmatrix} R^w_1 & p^w_1 \\ 0 & 1 \end{bmatrix} \begin{bmatrix} d_{12}\hat{v}^1_{12} \\ 1 \end{bmatrix} \tag{6}$$

Similarly, the reflected ray from the second mirror has direction:

$$\hat{v}^2_{2t} = H^2_2 \left(R^w_2\right)^{-1} R^w_1 \hat{v}^1_{12} \tag{7}$$

And intersects the target plane after a distance d_{2t}:

$$d_{2t} = (o_t - o_2)^T e^t_3 / \left(R^w_2 \hat{v}^2_{2t}\right)^T e^t_3 \tag{8}$$

Finally, p^w_t, the location of the laser spot on the target plane is given by:

$$p^w_t = \begin{bmatrix} R^w_2 & p^w_2 \\ 0 & 1 \end{bmatrix} \begin{bmatrix} d_{2t}\hat{v}^2_{2t} \\ 1 \end{bmatrix} \tag{9}$$

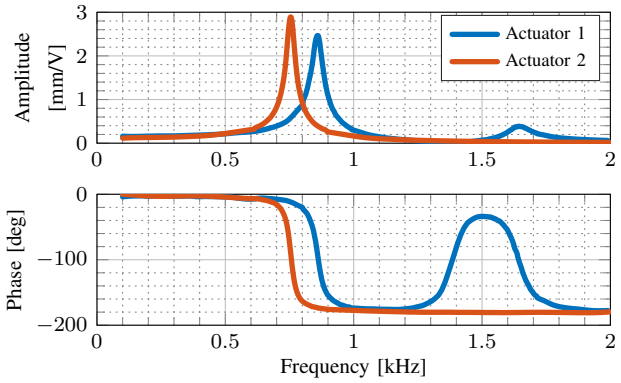

Fig. 7: Frequency response of the actuator-transmission-mirror subsystems. Measurements were taken at the tips of the actuators.

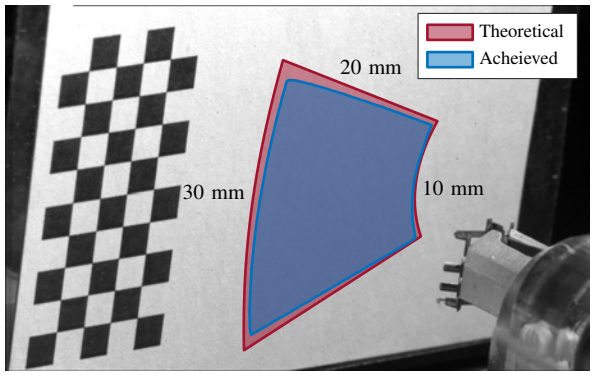

Fig. 8: Laser spot position tracking setup, as viewed from the high speed camera. Theoretical and achieved field of view from a 20 mm standoff distance are shown.

V. Results

To validate the crank slider kinematic model (1), mirror angle and actuator displacement were measured as a function of actuator voltage. Mirror angle was measured under static voltage input using a high-zoom inspection camera (PixeLINK PL-B741F) and actuator displacement was measured under a 1 Hz quasi-static cyclic input using a laser Doppler vibrometer (Polytec PSV-500). In Fig. 6, measured and predicted mirror angles are plotted as a function of actuator inputs, with the theoretical values drawn from the measured actuator displacements at a given voltage. The results show that the model captures the broad behavior of the linkages. The measured data have mean absolute errors of $0.6°$ and $1.2°$ for the first and second mirrors, respectively.

In order to find safe bounds on input drive frequency, we conducted frequency analyses on both motion actuator-transmission-mirror subsystems. Data were collected under low-voltage white noise input using the same laser Doppler vibrometer. The results are shown in Fig. 7; as expected, both subsystems closely resemble second-order linear systems. The resonant frequencies of 850 Hz and 750 Hz accord with physical intuition: the free-beam resonance of the actuators ($\sim$1.6 kHz) has been reduced due to the added mass of the transmission.

To validate the beam steering capabilities of the device, we created a benchtop scanning arena incorporating a calibrated high-speed camera (Phantom v710) with a 200 mm macro lens and two non-flicker flood lights, all mounted on an optical table. The camera view is shown in Fig. 8 along with the grid used for image registration. One pixel corresponds to 50 µm in the image plane. We fixed our device on the optical table at our determined stand-off distance of 20 mm from the target.

We then calibrated the scanner by sweeping the voltage space and tracking the laser spot position. The overall field of view matches the model prediction well, as shown in Fig. 8. However, unmodeled compliance in the system and assembly misalignment created a slight scaling of the laser task space. Rather than adding extra degrees of freedom to our model and calibrating it, we chose to use a lookup-table approach for controlling the laser spot position.

This approach yields reasonable results for task-space trajectory following, as shown in Fig. 9. Three shapes, an "H", a "star", and a Lissajous figure, were drawn across a range of speeds. Each shape is shown at a base speed of 100 mm/s and at the highest speed that it could be reproduced before oscillations in the transmissions erode the device's tracking performance. Such oscillations emerge at 2 m/s in the "H" trajectory. Of the three shapes, the "H" is the most challenging due to the rapid, abrupt changes in the trajectory. The Lissajous figure is simplest, because the drive voltages on the actuators are smooth and nearly sinusoidal and thus suffer little loss in performance up to 7 m/s.

VI. Discussion

The prototype device satisfies the majority of the design requirements: field of view (slightly less than 10×20 mm), scanning speed (up to 7 m/s), and scanning device size (11 mm). Spot size validation was left for future work, in conjunction with integration of the high-powered diode laser, though preliminary experiments suggest that spot-size variation within the workspace is less than 10 %, which is an important, albeit secondary metric to absolute spot size.

The most significant errors in the trajectory following experiment occurred during vertical motions. Given the orientation of the device during those experiments, these motions were mostly generated by the second mirror. This is consistent with the insight that the second linkage transmission, as currently conceived, is slightly overconstrained because the linkage joint axes are not orthogonal to the plane in which the actuator tip displacement lies. Thus, the configuration of the linkage is determined by kinetics rather than kinematics. Future work will obviate this deficiency.

Another important next step is the integration of high-powered optics. To that end, miniature dielectric mirrors will need to be used to steer the high powered beam. Custom lenses of smaller diameter might need to be manufactured to decrease the diameter of the full device to 11 mm. Because we used readily available off-the-shelf optical components, the diameter of the optical subassembly of this device was 13 mm, though the scanning subsystem itself was 11 mm.

Before being ready for testing in clinical environments, additional questions of packaging and integration will need to be addressed. The somewhat fragile mechanical structure of the mirrors and linkages will need to be enclosed, and

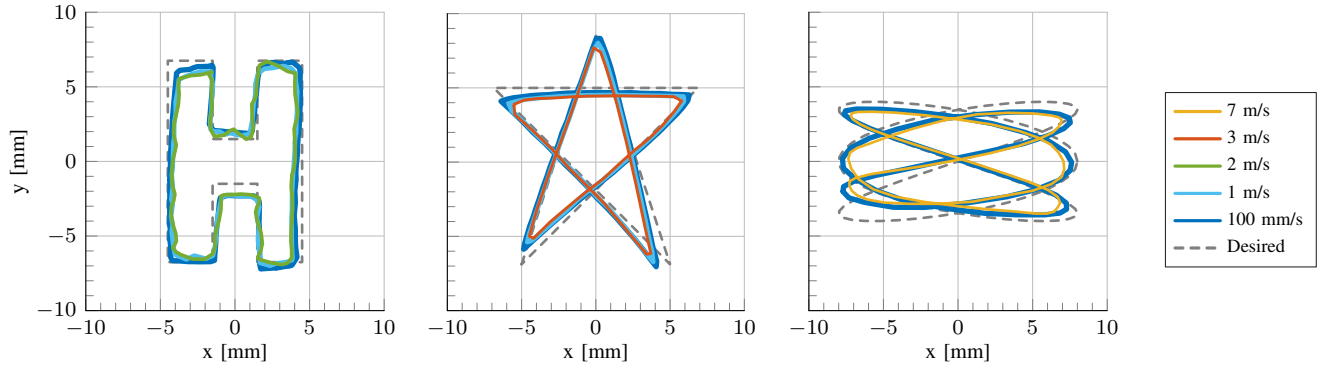

Fig. 9: Shapes drawn at different speeds demonstrate the open-loop trajectory following capabilities of the laser scanner. The high-speed performance of the system is shown through its repeatability across a range of commanded velocities.

the mirrors will need to be protected from fluid flow at the surgical site. We expect that this device would be used alongside existing transoral robotic tools for visualization and tissue retraction, so investigating task coordination with those tools will be an important component of future work.

VII. Conclusion

By combining the strengths of TORS and TLM, we anticipate that this approach has promise to improve the quality of care for pharyngeal and laryngeal cancers. It should allow for better access and exposure than with TLM alone, and higher incision quality than with TORS alone. The result should be streamlined procedures for surgeons and better functional outcomes for patients.

References

[1] R. L. Siegel, K. D. Miller, and A. Jemal, "Cancer statistics, 2018," *CA: A Cancer Journal for Clinicians*, vol. 68, no. 1, pp. 7–30.

[2] B. Ojo, E. M. Genden, M. S. Teng, K. Milbury, K. J. Misiukiewicz, and H. Badr, "A systematic review of head and neck cancer quality of life assessment instruments," *Oral oncology*, vol. 48, no. 10, pp. 923–937, 2012.

[3] A. K. Chaturvedi, E. A. Engels, R. M. Pfeiffer *et al.*, "Human papillomavirus and rising oropharyngeal cancer incidence in the united states," *Journal of clinical oncology*, vol. 29, no. 32, p. 4294, 2011.

[4] D. G. Pfister, S. A. Laurie, G. S. Weinstein *et al.*, "American society of clinical oncology clinical practice guideline for the use of larynx-preservation strategies in the treatment of laryngeal cancer," *Journal of clinical Oncology*, vol. 24, no. 22, pp. 3693–3704, 2006.

[5] F. C. Holsinger and R. S. Weber, "Swing of the surgical pendulum: a return to surgery for treatment of head and neck cancer in the 21st century?" *International Journal of Radiation Oncology Biology Physics*, vol. 69, no. 2, pp. S129–S131, 2007.

[6] M. S. Strong and G. J. Jako, "Laser surgery in the larynx early clinical experience with continuous CO2 laser," *Annals of Otology, Rhinology & Laryngology*, vol. 81, no. 6, pp. 791–798, 1972.

[7] M. Remacle, G. Lawson, M.-C. Nollevaux, and M. Delos, "Current state of scanning micromanipulator applications with the carbon dioxide laser," *Annals of Otology, Rhinology & Laryngology*, vol. 117, no. 4, pp. 239–244, 2008, pMID: 18478831.

[8] N. Simaan, R. Taylor, and P. Flint, "A dexterous system for laryngeal surgery," in *IEEE International Conference on Robotics and Automation*, 2004, pp. 351–357.

[9] G. S. Weinstein, B. W. O'Malley Jr, and N. G. Hockstein, "Transoral robotic surgery: supraglottic laryngectomy in a canine model," *The Laryngoscope*, vol. 115, no. 7, pp. 1315–1319, 2005.

[10] H. Poon, C. Li, W. Gao, H. Ren, and C. M. Lim, "Evolution of robotic systems for transoral head and neck surgery," *Oral oncology*, vol. 87, pp. 82–88, 2018.

[11] M. Ansarin, S. Zorzi, M. A. Massaro, M. Tagliabue, M. Proh, G. Giugliano, L. Calabrese, and F. Chiesa, "Transoral robotic surgery vs transoral laser microsurgery for resection of supraglottic cancer: a pilot surgery," *The International Journal of Medical Robotics and Computer Assisted Surgery*, vol. 10, no. 1, pp. 107–112, 2014.

[12] M. Karaman, T. Gün, B. Temelkuran, E. Aynacı, C. Kaya, and A. M. Tekin, "Comparison of fiber delivered CO2 laser and electrocautery in transoral robot assisted tongue base surgery," *European Archives of Oto-Rhino-Laryngology*, vol. 274, no. 5, pp. 2273–2279, 2017.

[13] M. Remacle, G. Lawson, M.-C. Nollevaux, and M. Delos, "Current state of scanning micromanipulator applications with the carbon dioxide laser," *Annals of Otology, Rhinology & Laryngology*, vol. 117, no. 4, pp. 239–244, 2008.

[14] S. Patel, M. Rajadhyaksha, S. Kirov, Y. Li, and R. Toledo-Crow, "Endoscopic laser scalpel for head and neck cancer surgery," in *Photonic Therapeutics and Diagnostics VIII*, vol. 8207. International Society for Optics and Photonics, 2012, p. 82071S.

[15] O. Ferhanoglu, M. Yildirim, K. Subramanian, and A. Ben-Yakar, "A 5-mm piezo-scanning fiber device for high speed ultrafast laser microsurgery," *Biomedical Optics Express*, vol. 5, no. 7, pp. 2023–2036, 2014.

[16] A. Acemoglu, D. Pucci, and L. S. Mattos, "Design and control of a magnetic laser scanner for endoscopic microsurgeries," *IEEE/ASME Transactions on Mechatronics*, vol. 24, no. 2, pp. 527–537, 2019.

[17] R. Renevier, B. Tamadazte, K. Rabenorosoa, L. Tavernier, and N. Andreff, "Endoscopic laser surgery: design, modeling and control," *IEEE/ASME Transactions on Mechatronics*, vol. 22, no. 1, pp. 99–106, 2017.

[18] P. S. Sreetharan, J. P. Whitney, M. D. Strauss, and R. J. Wood, "Monolithic fabrication of millimeter-scale machines," *Journal of Micromechanics and Microengineering*, vol. 22, no. 5, p. 055027, 2012.

[19] N. T. Jafferis, M. J. Smith, and R. J. Wood, "Design and manufacturing rules for maximizing the performance of polycrystalline piezoelectric bending actuators," *Smart Materials and Structures*, vol. 24, no. 6, p. 065023, 2015.

[20] Y. Yan, A. E. Olszewski, M. R. Hoffman, P. Zhuang, C. N. Ford, S. H. Dailey, and J. J. Jiang, "Use of lasers in laryngeal surgery," *Journal of Voice*, vol. 24, no. 1, pp. 102 – 109, 2010.

[21] H. H. Arroyo, L. Neri, C. Y. Fussuma, and R. Imamura, "Diode Laser for Laryngeal Surgery: a Systematic Review," *International Archives of Otorhinolaryngology*, vol. 20, pp. 172 – 179, 06 2016.